Accepted Manuscript

First principle calculation of helium in $La_2Zr_2O_7$: Effects on structural, electronic properties and radiation tolerance

C.G. Liu, Y.H. Li, Y.D. Li, L.Y. Dong, J. Wen, D.Y. Yang, Q.L. Wei, P. Yang

PII: S0022-3115(17)31047-4

DOI: 10.1016/j.jnucmat.2017.12.024

Reference: NUMA 50689

To appear in: *Journal of Nuclear Materials*

Received Date: 22 July 2017

Revised Date: 11 October 2017

Accepted Date: 13 December 2017

Please cite this article as: C.G. Liu, Y.H. Li, Y.D. Li, L.Y. Dong, J. Wen, D.Y. Yang, Q.L. Wei, P. Yang, First principle calculation of helium in $La_2Zr_2O_7$: Effects on structural, electronic properties and radiation tolerance, *Journal of Nuclear Materials* (2018), doi: 10.1016/j.jnucmat.2017.12.024.

First principle calculation of helium in $La_2Zr_2O_7$: effects on structural, electronic properties and radiation tolerance

C. G. Liu, Y. H. Li*, Y. D. Li, L. Y. Dong, J. Wen, D. Y. Yang, Q. L. Wei, P. Yang

School of Nuclear Science and Technology, Lanzhou University, Lanzhou, 730000, China

Abstract:

First principle calculations based on density functional theory have been employed to study structural effects of trapping helium in $La_2Zr_2O_7$ pyrochlore. Lattice swelling and the distortion of unit cell have been found in He-$La_2Zr_2O_7$ systems. By analyzing the electronic structures and chemical bonding of He-$La_2Zr_2O_7$ systems, weak repulsive and attractive chemical interactions of helium in $La_2Zr_2O_7$ pyrochlore have been observed. The formation energies have been calculated to assess the relative stability of various helium interstitial configurations and the results show that the octahedral interstitial site is the most stable structure. The cation antisite defect formation energies and the *x* positional parameter for 48*f*-site oxygen are calculated to predict the radiation resistence of He-$La_2Zr_2O_7$ systems. The results indicate that the presence of low concentration of He interstitials may increase the radiation resistance of $La_2Zr_2O_7$ pyrochlore.

Keywords:

Density functional theory; $La_2Zr_2O_7$ pyrochlore; Helium interstitial; Formation energy;

1. Introduction

Nuclear energy gets extensive development worldwide as a clean energy, which can solve the ecological environment problems caused by the over exploitation of fossil fuels, but it also creates challenges. The most serious one is dealing with high-level nuclear waste in reasonable ways [1-5]. $La_2Zr_2O_7$ pyrochlore has been proposed as a potential superior host phase for the long-lived transuranic (TRU) elements in nuclear waste, because it possesses high chemical durability, good thermal stability, low leach rate and the enhanced radiation tolerance after TRU elements incorporated [6-9]. In recent decades, many of experimental and theoretical investigations involving $La_2Zr_2O_7$ pyrochlore have been carried out to evaluate the radiation stability and the solubility of actinides in it [9-17]. For example, Lian *et al.* [16] argued that there was a close correlation between the radiation resistance of $La_2Zr_2O_7$ and its deviation from the ideal fluorite structure. Besides, the cation antisite formation energy has been introduced to predict the disordering extent and then assess the radiation tolerance of $La_2Zr_2O_7$ [16, 18, 19]. Cerium has been used as a nonradioactive surrogate for plutonium to investigate

*Corresponding author. Tel.: +86 138 9362 2587
E-mail address: liyuhong@lzu.edu.cn

the solubility of actinides in $La_2Zr_2O_7$. The density functional theory (DFT) calculation carried by Wang *et al*. [15] has demonstrated that cerium was soluble in $La_2Zr_2O_7$ pyrochlore, which is consistent with the experimental study of Lian *et al.*[20]. They also suggested that $La_2Zr_2O_7$ might be more favorable than $Gd_2Zr_2O_7$ in immobilizing actinide wastes. Recently, Xiao *et al.* [14] studied plutonium accommodation in $La_2Zr_2O_7$ by DFT plus Hubbard U method. Their results show that Pu could be incorporated into both La and Zr lattice sites, which is in agreement with the research of Kulkarni *et al*. [13] in experiment. They have also concluded that the incorporation of Pu in $La_2Zr_2O_7$ can enhance its radiation tolerance.

In all these discussions, however, the behavior of helium atom in pyrochlore is scarcely reported. Helium accumulation due to α-decay processes from plutonium and other minor actinides for hundreds of thousands of years can result in structural changes and then alter the chemical properties of immobilization matrix [21-23]. Until recently, Taylor *et al*. [22, 23] studied the combined effects of radiation damage and He accumulation on bubble nucleation in $Gd_2Zr_2O_7$ and $Gd_2Ti_2O_7$ pyrochlores. They concluded that lattice swelling occurred after irradiation with Au^{3+} and He^{+} ion in $Gd_2Zr_2O_7$. He bubbles were larger in a crystalline $Gd_2Ti_2O_7$ matrix than in the amorphous matrix. In addition, structural and electronic effects of helium interstitials in $Y_2Ti_2O_7$ pyrochlore, which is a primary precipitate phase in nano-structured ferritic alloys (NFAs) for fission and fussion energy applications [24], have been reported by Danielson *et al.*[25]. They found the stable octahedral helium interstitial position and changes of chemical bond characteristics caused by the presence of interstitial helium in $Y_2Ti_2O_7$ by first principle calculation. Yang *et al.* [24] listed several significant helium interstitial configurations in $Y_2Ti_2O_7$ pyrochlore and compared the relative stability of trapping helium in NFAs.

Enlightened by all above results, first principle method based on density functional theory has been employed to calculate and describe the behavior of helium in $La_2Zr_2O_7$ pyrochlore. In some sense, this work will provide guidence for further experiment and evaluate the performance of $La_2Zr_2O_7$ as a candidate immobilization matrix at the atomic level. In Section 2, the details of the calculations are presented. Section 3 provides the results and discussion of this work, which includes structural and electronic effects of helium interstitials, formation energies and cation antisite defect formation energies of He-$La_2Zr_2O_7$ systems. Finally, conclusions and summaries are given in Section 4.

2. Computational method

All the density functional theory (DFT) calculations are performed with the Vienna *ab initio* Simulation Package (VASP) [26-29] in conjunction with the projector augmented wave (PAW) method [30, 31]. The generalized gradient approximation (GGA) parameterized by Perdew-Burke-Enrzerhof (PBE) [32, 33] has been employed to describe exchange-correlation effects and the behavior of helium in pyrochlores accurately [25, 34, 35]. Pseudopotentials with the valence configurations $1s^2$ for He, $5s^25p^65d^16s^2$ for La, $4s^24p^64d^25s^2$ for Zr and $2s^22p^4$ for O have been used. To get

converged results, a plane wave cutoff energy is set as 478.9 eV and the 4×4×4 *k*-points for the He-$La_2Zr_2O_7$ system with a Monkhorst-Pack scheme have been used to sample Brillouin zone. Each composition is fully allowed to relax on both volume and shape until the total energy and total force are converged to 10^{-5}eV and 0.01eV/Å. The charge transfer and chemical bonds in He-$La_2Zr_2O_7$ systems have been analyzed by the Bader charge analysis code [36-38] and the VESTA software [39].

3. Results and discussion

3.1 Crystal structure and structural properties of helium in $La_2Zr_2O_7$

The $A_2B_2O_7$ pyrochlore with space group F$d\bar{3}$m (No. 227) includes eight molecules per unit cell. It consists of four crystallographically nonequivalent kinds of atom: A (here, A = La), B (here, B = Zr), O and O' that occupy the 16*d* (0.5, 0.5, 0.5), 16*c* (0, 0, 0), 48*f* (*x*, 0.125, 0.125) and 8*b* (0.375, 0.375, 0.375) Wyckoff positions, respectively. The pyrochlore structure can be completely described by two independent structural parameters: the lattice parameter, a_0 and the internal atomic parameter, x_{O48f} [40]. Generally, the x_{O48f} positional parameter is an important measure of the degree of structural disorder and its value limits between 0.3125 and 0.375 in pyrochlore. For *x*=0.3125, the B ion has a perfect octahedral coordination while the A ion will be situated in a distorted cubic coordination and the system is a perfectly ordered pyrochlore structure. When *x*=0.375, the B ion will be at the center of a trigonal antiprism whereas the polyhedron of A-sites will change to a regular cube and the system has been disordered to the fluorite structure [40]. Pyrochlores with the higher value of x_{O48f} are more easily transformed into disordered fluorite structure and the structure will be more resistant to amorphization under irradiation [15, 41, 42]. For pure $La_2Zr_2O_7$ pyrochlore (Fig. 1(a)), the optimized lattice constant a_0, the internal atomic parameter x_{O48f} and the bond distance of <La-O_{48f}>, <La-O_{8b}> and <Zr-O_{48f}> are calculated and listed in Table. 1, which are in good agreement with other calculation and experiment results [40, 43].

To investigate the behavior of single helium interstitial in $La_2Zr_2O_7$ pyrochlore, the systems with five types of helium interstitial sites (Fig. 1(b)-(f)) have experienced a full structural relaxation and the structural changes caused by helium interstitial have been found. Particularly, the helium interstitial at the middle position of two Zr atoms relaxes into the tetrahedral position, which can be concluded by comparing the volume changes summarized in Table. 2 and the formation energies performed in Section 3.2. Because of these, the so called "Zr-Zr" interstitial will be treated as the tetrahedral interstitial in all the following analysis. Comparing with the pure $La_2Zr_2O_7$ pyrochlore, the volume of He-$La_2Zr_2O_7$ system increases by 2.38% (La-La interstitial site), 3.18% (O-O interstitial site), 2.54% (Octahedral interstitial site) and 2.54% (Tetrahedral interstitial site), respectively. From Table. 2, the single helium interstitial in $La_2Zr_2O_7$ increases the value of x_{O48f} and the He-$La_2Zr_2O_7$ systems are closer to disordered fluorite structure. These

results suggest that the existence of helium interstitial in $La_2Zr_2O_7$ may cause lattice swelling and enhance the resistance to irradiation induced amorphization.

3.2 **Formation energies of helium interstitials**

Formation energies, which are used to assess the relative stabilities of interstitial atom in compounds [24, 25, 35, 44], have been calculated in this part. The formation energies of helium atom at interstitial sites in $La_2Zr_2O_7$ are obtained using the expression:[35]

$$E_f^{He(Int)} = E_{He-La_2Zr_2O_7} - E_{La_2Zr_2O_7} - E_{He} \quad (1)$$

Here, $E_{He-La_2Zr_2O_7}$ are total energies of the relaxed $La_2Zr_2O_7$ configurations including an interstitial helium atom, $E_{La_2Zr_2O_7}$ is the total energy of the pure $La_2Zr_2O_7$ supercell. E_{He} is the ground state energy of an isolated helium atom. The formation energies of helium occupying the pre-existing vacancy (La-vacancy, Zr-vacancy, O_{8b}-vacancy and O_{48f}-vacancy, respectively) sites in $La_2Zr_2O_7$ are defined using the equation:[35]

$$E_f^{He(Vac)} = E_{He+Vac} - E_{Vac} - E_{He} \quad (2)$$

Where E_{He+Vac} are total energies of a single He atom at the pre-existing vacancy site in $La_2Zr_2O_7$ supercell, E_{Vac} are total energies of $La_2Zr_2O_7$ supercell containing a pre-existing vacancy.

For the formation energies of helium atom at interstitial sites in $La_2Zr_2O_7$, as listed in Table 3, the octahedral interstitial site with the lowest formation energy of $E_f^{He(Int)} = 1.6$ eV is the most stable configuration. The O-O interstitial site has the highest formation energy (2.69 eV) and is the least stable configuration, which is consistent with the largest volumetric strain (Table. 2) induced by helium occupying this location. Further, these results indicate that helium atoms are more easily trapped in the octahedral interstitial sites in $La_2Zr_2O_7$ pyrochlore.

The vacancy defects will be presented in pyrochlore under irradiation [45-47] and helium atoms can be trapped in these vacancy defects. The formation energies of helium at substitutional sites have been investigated and the results are illustrated in Table 3. It is found that the system with helium atom locating at La vacancy has the lowest formation energy (0.33 eV), meaning there is a stronger interaction between helium atom with La vacancy than other sites and helium atoms can be easily trapped by La vacancy in $La_2Zr_2O_7$ pyrochlore. In addition, comparing $E_f^{He(Vac)}$ with $E_f^{He(Int)}$ in Table 3, it can be found that helium atoms prefer inhabiting La-vacancy (0.33 eV) and Zr-vacancy (0.37 eV) to occupying O_{48f}-vacancy (1.57 eV) site and interstitial sites (1.6-2.69 eV), the O_{8b}-vacancy site (3.11 eV) may be the last choice for single helium atom.

3.3 **Cation antisite defect formation energies of He-$La_2Zr_2O_7$ systems**

To understand the impact of helium interstitials in the radiation tolerance of He-$La_2Zr_2O_7$ systems, the cation antisite defect formation energies are performed. The formation energies are obtained by:

$$E_f^{CA} = E_{tot}^{CA} - E_{tot} \quad (3)$$

Where E_{tot}^{CA} are the total energies of the He-$La_2Zr_2O_7$ supercells with a cation antisite defect which is formed by exchange of the neighboring La and Zr atom. E_{tot} are the total energies of He-$La_2Zr_2O_7$ supercells. Taylor *et al*. [22] have experimentally determined that the critical He concentration required to nucleate bubbles > 1 nm in diameter in bulk $Gd_2Zr_2O_7$ is 4.6 at.%. Until now, there is no relevant report about the critical concentration of He formation in $La_2Zr_2O_7$. Because helium atoms prefer occupying octahedral interstitial sites, the cation antisite defect formation energies of He-$La_2Zr_2O_7$ systems are calculated based on the $La_2Zr_2O_7$ supercells with the maximal He content up to ~3.3 at.% in octahedral interstitial sites and without He bubbles formation in the configurations. The various configurations are shown in Fig. 2. The results summarized in Table. 4 show that the cation antisite defect formation energies of He-$La_2Zr_2O_7$ systems are lower than that of pure $La_2Zr_2O_7$. Pyrochlores with lower cation antisite defect formation energies will be more easily disordered to the defect fluorite structure that is more resistant to amorphization under irradiation[18, 19, 48-50]. For these reason, we predict that the presence of low concentration of He interstitials (below the critical concentration of He bubbles) may increase the radiation resistance of $La_2Zr_2O_7$ pyrochlore. From another point of view, helium interstitials can result in the distortion of unit cell and bring the configuration closer to fluorite structure. For example, the least stable structure of He in O-O interstitial site (with highest formation energy 2.69 eV) has the largest x_{O48f} and lowest cation antisite defect formation energy (0.78 eV).

3.4 Electronic structures and chemical bonding

The electronic properties of compounds provide physical insight into the structural and physical properties. The Bader charge analysis [36-38], the electron localization function (ELF) [51] and the partial density of states (PDOS) are always performed to investigate the electronic structures of compounds. Recently, the interaction of He with $Y_2Ti_2O_7$ pyrochlore has been investigated using these electronic structure calculation methods [25, 35]. To the best of our knowledge, few electronic structural analyses have been reported for helium absorption in pyrochlore. In this study, we have systematically explored the electronic properties of pure $La_2Zr_2O_7$ and He occupied different interstitial sites in $La_2Zr_2O_7$ pyrochlore by using above analysis methods (Bader charge analysis, ELF and PDOS). Fig. 3 presents the density of states close to the Fermi level for the pure $La_2Zr_2O_7$ system. The valence bands are mainly contributed by the 2*p* orbitals of oxygen, and a minor contribution from the 4*d* orbitals of zirconium. The conduction bands are mainly composed by the Zr 4*d* orbitals hybridized with O 2*p*

orbitals. Besides, a stronger hybridization of Zr-4*d* and O-2*p* than that of La-5*d* and O-2*p* is obvious in the PDOS of $La_2Zr_2O_7$ pyrochlore. This result is in agreement with previous calculations by Pruneda *et al*. [43], Liu *et al*. [52]. To further investigate the chemical bonding of $La_2Zr_2O_7$, the Bader charge analysis and the ELF have been carried out. From Fig. 4, Bader charge for Zr ion (9.4471) is much larger than that of La ion (8.8801), indicating that the degree of covalency of the <Zr-O> bond is stronger than that of the <La-O> bond. Accordingly, the ELF, which can give quantitative picture on the chemical bonding and a convenient mathematical framework clarifying characterization of bonds [51], is shown in Fig. 4. An increase of ELF for Zr and a decrease for La also demonstrate that <Zr-O> bonds are more covalent than <La-O> bonds, similar to the calculations of $La_2Zr_2O_7$ reported by Terki *et al*.[53]. Fig. 5 shows the difference of the partial density of states (ΔPDOS) ($\Delta PDOS = PDOS_{\mathrm{He-La_2Zr_2O_7}} - PDOS_{La_2Zr_2O_7}$) for He in different interstitial sites. The positive values mean an increase, negative values indicate a decrease and zero means He-$La_2Zr_2O_7$ system has the same PDOS as the pure system. There are clear changes in La-*s*, La-*d*, Zr-*s*, Zr-*d* and O-*p* states, which indicate the significant changes in the <La-O> bonds and <Zr-O> bonds. Besides, the degree of covalency of the <Zr-O> bond is stronger than the <La-O> bond from the number of states per energy level. The ELF of helium interstitial at the midpoint of two lanthanum atoms and Bader charge of relative ions are illustrated in Fig. 6. The <La_8-O_{52}> and <La_{14}-O_{52}> bonds have become more covalent which is reflected by the charge of O_{52} decreasing from 7.3636 to 7.3180 and the charge of La_8 and La_{14} increasing from 8.8801 to 8.9062 and 8.8961, respectively. The decrease in the charge of Zr_1 from 9.4474 to 9.4288 and the increase in Zr_{15} from 9.4474 to 9.4718 show the <Zr_1-O_9> bond decreases in covalency while the <Zr_{15}-O_9> bond increases in covalency. The displacement of O_9 along [010] direction is founded by comparing the structure of this configuration before and after full relaxation, which reduces the distance between Zr_{15} atom and O_9 atom and enhances the covalency of <Zr_{15}-O_9> bond. Similarly, it results in the decrease of the covalency of the <Zr_1-O_9> bond. Besides, Fig. 6 points out that the Bader volume of O_9 decreases from 14094000 pm^3 to 13894900 pm^3. All the results indicate that the helium has a significant interaction with oxygen atom. Dissymmetrical changes in <La-O> bonds have also been observed in O-O interstitial configuration. From Fig. 7, the charge of O_{26} decreases from 7.3304 to 7.3238 while the charge of O_{44} increases from 7.3303 to 7.3324, which demonstrates an increase in the covalency of <La_9-O_{26}> bond and a decrease in the covalency of <La_9-O_{44}> bond, which is attributed to the change of bond distance, bond angle and the distortion of the unit cell [25]. The same phenomenon also appears in octahedral interstitial (Fig. 8) and tetrahedral (Fig. 9) configuration. In the octahedral configuration, there are increases in covalency of <La_3-O_{55}>, <La_{11}-O_{55}>, <La_{11}-O_{50}>, <Zr_{10}-O_8> bonds and decreases in covalency of <La_3-O_{31}>, <La_{11}-O_5>, <La_{11}-O_{31}>, <Zr_4-O_8>. These changes may be caused by O_8 atom displacing towards Zr_{10} atom and O_{55} atom displacing towards La_{11} atom. In the tetrahedral configuration, due to the interaction between helium with

oxygen, the displacement of O_{39} in $[\bar{1}00]$ direction has been found, which may be the reason of a decrease in covalency of <Zr_1-O_{39}> and <Zr_{15}-O_{39}> bond.

From the above discussion, it can be concluded that the He absorption in $La_2Zr_2O_7$ pyrochlore is weak repulsive and attractive chemical interactions rather than physical processes, which is consistent with the research of He absorption in $Y_2Ti_2O_7$ pyrochlore [25, 35]. Besides local changes of electronic structures and chemical bonding caused by helium interstitials, we also calculated average La charge and average Zr charge in $La_2Zr_2O_7$ to evaluate the covalency of <La-O> bond and <Zr-O> bond from the integral perspective, which are listed in Table. 5. The result shows that a minor decrease in average Zr charge and a minor increase in average La charge do exist. Further, there is a net increase in the covalency of <La-O> bond and decrease in the covalency of <Zr-O> bond in He-$La_2Zr_2O_7$ systems. The covalency of chemical bond has been regarded as a proposed criterion to predict the resistance to amorphization of pyrochlore. The ability to form a covalent network leads to damage stabilization and makes a material amorphizable by radiation damage. Low covalency, on the other hand, results in higher resistance [54]. Combining with our previous results of anti-site defect formation energies in Section 3.3, <Zr-O> bonds play a more dominant role than <La-O> bonds in determining the radiation tolerance of He-$La_2Zr_2O_7$ systems.

4. Conclusion

To conclude, we have systematically studied structural and electronic effects of helium interstitials, formation energies and cation antisite defect formation energies of He-$La_2Zr_2O_7$ systems based on density functional theory. We found that the existence of helium interstitial in $La_2Zr_2O_7$ may cause lattice swelling and the distortion of unit cell. The result of formation energies shows that the octahedral interstitial site is the most stable helium interstitial site. The decreased cation antisite defect formation energies and the increased x_{O48f} indicate that the configuration will be more easily disordered to the defect fluorite structure after the presence of low concentration of He interstitials in $La_2Zr_2O_7$. By analyzing the electronic structures and chemical bonding of He-$La_2Zr_2O_7$ systems, we pointed out that the He absorptions in $La_2Zr_2O_7$ pyrochlore are weak repulsive and attractive chemical interactions rather than physical processes and <Zr-O> bonds play a more dominating role than <La-O> bonds in determining the radiation tolerance of $La_2Zr_2O_7$ pyrochlore.

Acknowledgments

This work was supported by the National Natural Science Foundation of China. (No. 11475076, 51471160, 11775102) and the Fundamental Research Funds for the Central Universities of China (Lanzhou University lzujbky-2017-14).

References

[1] D.H. Chestnut, Ten years of experience with accidental dural puncture and post-dural puncture headache in a tertiary obstetric anaesthesia department, Yearbook of Anesthesiology and Pain Management, 2009 (2009) 252-253.

[2] M.Z. Jacobson, Review of solutions to global warming, air pollution, and energy security, Energy & Environmental Science, 2 (2009) 148-173.

[3] N. Armaroli, V. Balzani, Towards an electricity-powered world, Energy & Environmental Science, 4 (2011) 3193-3222.

[4] R.W. Grimes, W.J. Nuttall, Generating the Option of a Two-Stage Nuclear Renaissance, Science, 329 (2010) 799.

[5] A. Chroneos, M.J.D. Rushton, C. Jiang, L.H. Tsoukalas, Nuclear wasteform materials: Atomistic simulation case studies, Journal of Nuclear Materials, 441 (2013) 29-39.

[6] I. Hayakawa, H. Kamizono, Durability of an $La_2Zr_2O_7$ waste form in water, Journal of Materials Science, 28 (1993) 513-517.

[7] H. Kamizono, I. Hayakawa, S. Muraoka, Durability of Zirconium-Containing Ceramic Waste Forms in Water, Journal of the American Ceramic Society, 74 (1991) 863-864.

[8] I. Hayakawa, H. Kamizono, Durability of an $La_2Zr_2O_7$ waste form containing various amounts of simulated HLW elements, Journal of Nuclear Materials, 202 (1993) 163-168.

[9] J. Lian, L.M. Wang, R.G. Haire, K.B. Helean, R.C. Ewing, Ion beam irradiation in $La_2Zr_2O_7$–$Ce_2Zr_2O_7$ pyrochlore, Nuclear Instruments and Methods in Physics Research Section B: Beam Interactions with Materials and Atoms, 218 (2004) 236-243.

[10] K. Holliday, S. Finkeldei, S. Neumeier, C. Walther, D. Bosbach, T. Stumpf, TRLFS of Eu^{3+} and Cm^{3+} doped $La_2Zr_2O_7$: A comparison of defect fluorite to pyrochlore structures, Journal of Nuclear Materials, 433 (2013) 479-485.

[11] S. Yamazaki, T. Yamashita, T. Matsui, T. Nagasaki, Thermal expansion and solubility limits of plutonium-doped lanthanum zirconates, Journal of Nuclear Materials, 294 (2001) 183-187.

[12] D.J. Gregg, Y. Zhang, S.C. Middleburgh, S.D. Conradson, G. Triani, G.R. Lumpkin, E.R. Vance, The incorporation of plutonium in lanthanum zirconate pyrochlore, Journal of Nuclear Materials, 443 (2013) 444-451.

[13] N.K. Kulkarni, S. Sampath, V. Venugopal, Preparation and characterisation of Pu-pyrochlore: $[La_{1-x}Pu_x]_2Zr_2O_7$ (x=0–1), Journal of Nuclear Materials, 281 (2000) 248-250.

[14] H.Y. Xiao, M. Jiang, F.A. Zhao, Z.J. Liu, X.T. Zu, Thermal and mechanical stability, electronic structure and energetic properties of Pu-containing pyrochlores: $La_{2-y}Pu_yZr_2O_7$ and $La_2Zr_{2-y}Pu_yO_7$ ($0 \le y \le 2$), Journal of Nuclear Materials, 466 (2015) 162-171.

[15] X.J. Wang, H.Y. Xiao, X.T. Zu, W.J. Weber, A DFT+U study of cerium solubility in $La_2Zr_2O_7$, Journal of Nuclear Materials, 424 (2012) 69-74.

[16] J. Lian, L.M. Wang, J. Chen, R.C. Ewing, K.V.G. Kutty, Heavy Ion Irradiation of Zirconate Pyrochlores, MRS Proceedings, 713 (2011).

[17] J. Lian, X. Zu, K.G. Kutty, J. Chen, L. Wang, R. Ewing, Ion-irradiation-induced amorphization of $La_2Zr_2O_7$ pyrochlore, Physical Review B, 66 (2002) 054108.

[18] Y. Li, P.M. Kowalski, G. Beridze, A.R. Birnie, S. Finkeldei, D. Bosbach, Defect formation energies in $A_2B_2O_7$ pyrochlores, Scripta Materialia, 107 (2015) 18-21.

[19] K. Sickafus, L. Minervini, R. Grimes, J. Valdez, M. Ishimaru, F. Li, K. McClellan, T. Hartmann, Radiation tolerance of complex oxides, Science, 289 (2000) 748-751.

[20] J. Lian, L. Wang, R. Haire, K. Helean, R. Ewing, Ion beam irradiation in $La_2Zr_2O_7$–$Ce_2Zr_2O_7$ pyrochlore, Nuclear Instruments and Methods in Physics Research Section B: Beam Interactions with Materials and Atoms, 218 (2004) 236-243.

[21] W.J. Weber, A. Navrotsky, S. Stefanovsky, E.R. Vance, E. Vernaz, Materials Science of High-Level Nuclear Waste Immobilization, MRS Bulletin, 34 (2011) 46-53.

[22] C.A. Taylor, M.K. Patel, J.A. Aguiar, Y. Zhang, M.L. Crespillo, J. Wen, H. Xue, Y. Wang, W.J. Weber, Bubble formation and lattice parameter changes resulting from He irradiation of defect-fluorite $Gd_2Zr_2O_7$, Acta Materialia, 115 (2016) 115-122.

[23] C.A. Taylor, M.K. Patel, J.A. Aguiar, Y. Zhang, M.L. Crespillo, J. Wen, H. Xue, Y. Wang, W.J. Weber, Combined effects of radiation damage and He accumulation on bubble nucleation in $Gd_2Ti_2O_7$, Journal of Nuclear Materials, 479 (2016) 542-547.

[24] L. Yang, Y. Jiang, G. Robert Odette, T. Yamamoto, Z. Liu, Y. Liu, Trapping helium in $Y_2Ti_2O_7$ compared to in matrix iron: A first principles study, Journal of Applied Physics, 115 (2014) 143508.

[25] T. Danielson, C. Hin, Structural and electronic effects of helium interstitials in $Y_2Ti_2O_7$: A first-principles study, Journal of Nuclear Materials, 452 (2014) 189-196.

[26] G. Kresse, J. Hafner, Ab initio, Physical Review B, 47 (1993) 558-561.

[27] G. Kresse, J. Hafner, Ab initio, Physical Review B, 49 (1994) 14251-14269.

[28] G. Kresse, J. Furthmüller, Efficiency of ab-initio total energy calculations for metals and semiconductors using a plane-wave basis set, Computational Materials Science, 6 (1996) 15-50.

[29] G. Kresse, J. Furthmüller, Efficient iterative schemes for ab initio total-energy calculations using a plane-wave basis set, Physical Review B, 54 (1996) 11169-11186.

[30] P.E. Blöchl, Projector augmented-wave method, Physical Review B, 50 (1994) 17953-17979.

[31] G. Kresse, D. Joubert, From ultrasoft pseudopotentials to the projector augmented-wave method, Physical Review B, 59 (1999) 1758-1775.

[32] J.P. Perdew, K. Burke, M. Ernzerhof, Generalized Gradient Approximation Made Simple [Phys. Rev. Lett. 77, 3865 (1996)], Physical Review Letters, 78 (1997) 1396-1396.

[33] J.P. Perdew, K. Burke, M. Ernzerhof, Generalized Gradient Approximation Made Simple, Physical Review Letters, 77 (1996) 3865-3868.

[34] T. Danielson, E. Tea, C. Hin, Ab initio investigation of helium in $Y_2Ti_2O_7$: Mobility and effects on mechanical properties, Journal of Nuclear Materials, 477 (2016) 215-221.

[35] B. Tsuchiya, T. Yamamoto, K. Ohsawa, G.R. Odette, First-principles calculation of formation energies and electronic structures of hydrogen defects at tetrahedral and octahedral interstitial sites in pyrochlore-type $Y_2Ti_2O_7$ oxide, Journal of Alloys and Compounds, 678 (2016) 153-159.

[36] W. Tang, E. Sanville, G. Henkelman, A grid-based Bader analysis algorithm without lattice bias, Journal of Physics: Condensed Matter, 21 (2009) 084204.

[37] E. Sanville, S.D. Kenny, R. Smith, G. Henkelman, Improved grid-based algorithm for Bader charge allocation, Journal of Computational Chemistry, 28 (2007) 899-908.

[38] G. Henkelman, A. Arnaldsson, H. Jónsson, A fast and robust algorithm for Bader decomposition of charge density, Computational Materials Science, 36 (2006) 354-360.

[39] K. Momma, F. Izumi, for three‐dimensional visualization of crystal, volumetric and morphology data, Journal of Applied Crystallography, 44 (2011) 1272–1276.

[40] M.A. Subramanian, G. Aravamudan, G.V. Subba Rao, Oxide pyrochlores — A review, Progress in Solid State Chemistry, 15 (1983) 55-143.
[41] J. Lian, J. Chen, L.M. Wang, R.C. Ewing, J.M. Farmer, L.A. Boatner, K.B. Helean, Radiation-induced amorphization of rare-earth titanate pyrochlores, Physical Review B, 68 (2003).
[42] J. Lian, L.M. Wang, J. Chen, R.C. Ewing, K.V.G. Kutty, Heavy Ion Irradiation of Zirconate Pyrochlores, Mrs Online Proceeding Library, 713 (2001).
[43] J.M. Pruneda, E. Artacho, First-principles study of structural, elastic, and bonding properties of pyrochlores, Physical Review B, 72 (2005).
[44] F. Gao, H.Y. Xiao, Y.G. Zhou, R. Devanathan, S.Y. Hu, Y. L. Li, X. Sun, M.A. Khaleel, Ab initio study of defect properties in YPO_4, Computational Materials Science, 54 (2012) 170-175.
[45] W.J. Weber, R.C. Ewing, C.R.A. Catlow, d.L.R. Diaz, T, L.W. Hobbs, C. Kinoshita, H. Matzke, A.T. Motta, M. Nastasi, E.H.K. Salje, Radiation effects in crystalline ceramics for the immobilization of high-level nuclear waste and plutonium, Journal of Materials Research, 13 (1998) 1434-1484.
[46] R.C. Ewing, W.J. Weber, J. Lian, Nuclear waste disposal—pyrochlore ($A_2B_2O_7$): Nuclear waste form for the immobilization of plutonium and "minor" actinides, Journal of Applied Physics, 95 (2004) 5949-5971.
[47] A. Chartier, C. Meis, J.-P. Crocombette, L.R. Corrales, W.J. Weber, Atomistic modeling of displacement cascades in $La_2Zr_2O_7$ pyrochlore, Physical Review B, 67 (2003).
[48] L. Chen, X. Su, Y. Li, First-Principles Study on Cation-Antisite Defects of Stannate and Titanate Pyrochlores, OALib, 01 (2014) 1-8.
[49] Y. Xia, C.G. Liu, D.Y. Yang, J. Wen, H. Liu, P.C. Mu, Y.H. Li, Synthesis and radiation tolerance of $Lu_{2-x}Ce_xTi_2O_7$ pyrochlores, Journal of Nuclear Materials, 480 (2016) 182-188.
[50] Y.H. Li, B.P. Uberuaga, C. Jiang, S. Choudhury, J.A. Valdez, M.K. Patel, J. Won, Y.Q. Wang, M. Tang, D.J. Safarik, D.D. Byler, K.J. McClellan, I.O. Usov, T. Hartmann, G. Baldinozzi, K.E. Sickafus, Role of antisite disorder on preamorphization swelling in titanate pyrochlores, Phys Rev Lett, 108 (2012) 195504.
[51] A.D. Becke, K.E. Edgecombe, A simple measure of electron localization in atomic and molecular systems, The Journal of chemical physics, 92 (1990) 5397-5403.
[52] B. Liu, J.Y. Wang, Y.C. Zhou, T. Liao, F.Z. Li, Theoretical elastic stiffness, structure stability and thermal conductivity of $La_2Zr_2O_7$ pyrochlore, Acta Materialia, 55 (2007) 2949-2957.
[53] R. Terki, H. Feraoun, G. Bertrand, H. Aourag, Full potential linearized augmented plane wave investigations of structural and electronic properties of pyrochlore systems, Journal of Applied Physics, 96 (2004) 6482-6487.
[54] K. Trachenko, Understanding resistance to amorphization by radiation damage, Journal of Physics: Condensed Matter, 16 (2004) R1491-R1515.

Figure Captions:

Fig. 1 Configurations of various helium interstitial atom in $La_2Zr_2O_7$ pyrochlore. Site-related atom number is shown. The ivory, purple, green and red spheres represent the helium, lanthanum, zirconium and oxygen, respectively. (a) pure $La_2Zr_2O_7$ pyrochlore; (b) the helium interstitial at the midpoint of two lanthanum atoms (101

plane); (c) the helium interstitial at the midpoint of two zirconium atoms (100 plane); (d) the helium interstitial at the midpoint of two oxygen atoms; (e) the helium on the octahedral location; (f) the helium on the tetrahedral location.

Fig. 2 Configurations of various helium interstitials on the octahedral location. ((a)-He21; (b)-He22; (c)-He23; (d)-He31; (e)-He32).

Fig. 3 DOS distribution for pure $La_2Zr_2O_7$ pyrochlore.

Fig. 4 ELF (left) (e/Bohr^3) and Bader charge (right) for pure $La_2Zr_2O_7$.

Fig. 5 The difference of the partial density of states (ΔPDOS) for each helium interstitial configuration.

Fig. 6 ELF (left) (e/Bohr^3) and Bader charge (right) for the helium interstitial at the midpoint of two lanthanum atoms.

Fig. 7 ELF (left) (e/Bohr^3) and Bader charge (right) for the helium interstitial at the midpoint of two oxygen atoms.

Fig. 8 ELF (left) (e/Bohr^3) and Bader charge (right) for the helium on the octahedral location.

Fig. 9 ELF (left) (e/Bohr^3) and Bader charge (right) for the helium on the tetrahedral location.

Table Captions:

Table. 1 Calculated lattice constant, the *x* positional parameter for 48*f*-site oxygen and bond distance (Å), compared with available experimental and theoretical results.

Table. 2 Calculated the *x* positional parameter for 48*f*-site oxygen and volume for He-$La_2Zr_2O_7$ systems.

Table. 3 Calculated formation energies of helium atom at interstitial sites ($E_f^{He(Int)}$) and the pre-existing vacancy ($E_f^{He(Vac)}$).

Table.4 Cation antisite defect formaion energies for each helium interstitial configuration.

Table. 5 Calculated average La charge and average Zr charge in He-$La_2Zr_2O_7$ systems.

Table. 1 Calculated lattice constant, the *x* positional parameter for 48*f*-site oxygen and bond distance (Å), compared with available experimental and theoretical results.

$La_2Zr_2O_7$	present work	Other work	
		Exp. [40]	Theory [43]
a_0(Å)	10.797	10.805	10.724
x_{O48f}	0.3338	0.332	0.3314
La-O_{48f}(Å)	2.62	2.635	2.62
La-O_{8b}(Å)	2.34	2.339	2.32
Zr-O_{48f}(Å)	2.11	2.105	2.09

Table. 2 Calculated the *x* positional parameter for 48*f*-site oxygen and volume for He-$La_2Zr_2O_7$ systems

	x_{O48f}	Volume (nm^3)
$La_2Zr_2O_7$	0.3338	1.259
La-La	0.3599	1.289
O-O	0.3734	1.299
Zr-Zr	0.3339	1.290
Octahedral	0.3351	1.291
Tetrahedral	0.3372	1.291

Table. 3 Calculated formation energies of helium atom at interstitial sites ($E_f^{He(Int)}$) and the pre-existing vacancy ($E_f^{He(Vac)}$).

Formation energy (eV)	$E_f^{He(Int)}$					$E_f^{He(Vac)}$			
Site	La-La	O-O	Zr-Zr	Tet.	Oct.	La	Zr	O_{48f}	O_{8b}
Value	1.80	2.69	2.02	2.01	1.60	0.33	0.37	1.57	3.11

Table.4 Cation antisite defect formaion energies for each helium interstitial configuration.

Configuration	Cation antisite defect formation energy (eV)	Configuration	Cation antisite defect formation energy (eV)
$La_2Zr_2O_7$	2.410	**He21**	2.096
La-La	1.887	**He22**	1.953
O-O	0.780	**He23**	0.962
Oct.	1.931	**He31**	2.176
Tet.	2.317	**He32**	0.997

Table. 3 Calculated average La charge and average Zr charge in He-$La_2Zr_2O_7$ systems.

Configuration	Average La charge (e)	Average Zr charge (e)
$La_2Zr_2O_7$	8.880	9.447
La-La	8.907	9.439
O-O	8.902	9.437
Oct.	8.891	9.438
Tet.	8.876	9.440
He21	8.891	9.437
He22	8.896	9.436
He23	8.905	9.436
He31	8.889	9.436
He32	8.904	9.435

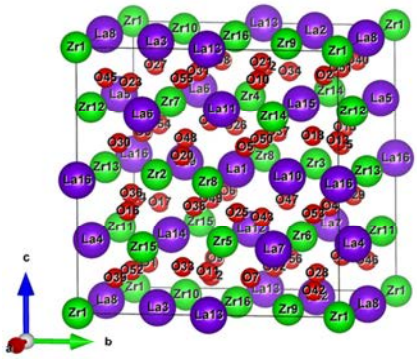

(a)

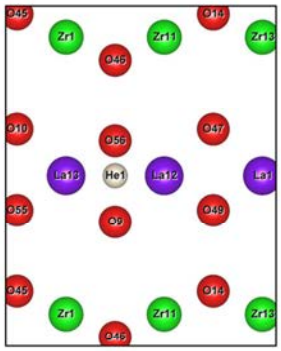

(b)

(c)

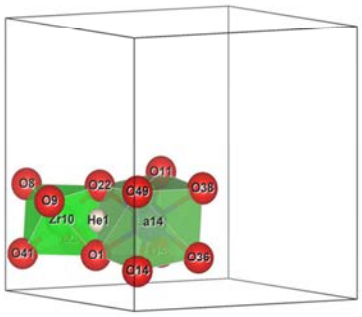

(d)

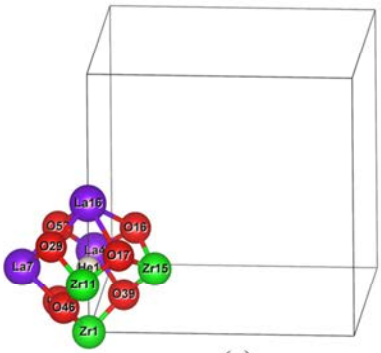

(e)

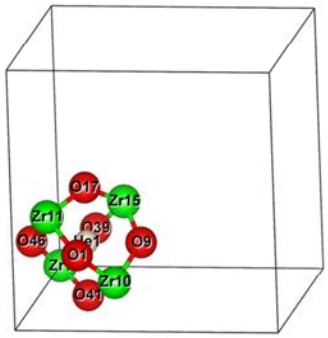

(f)

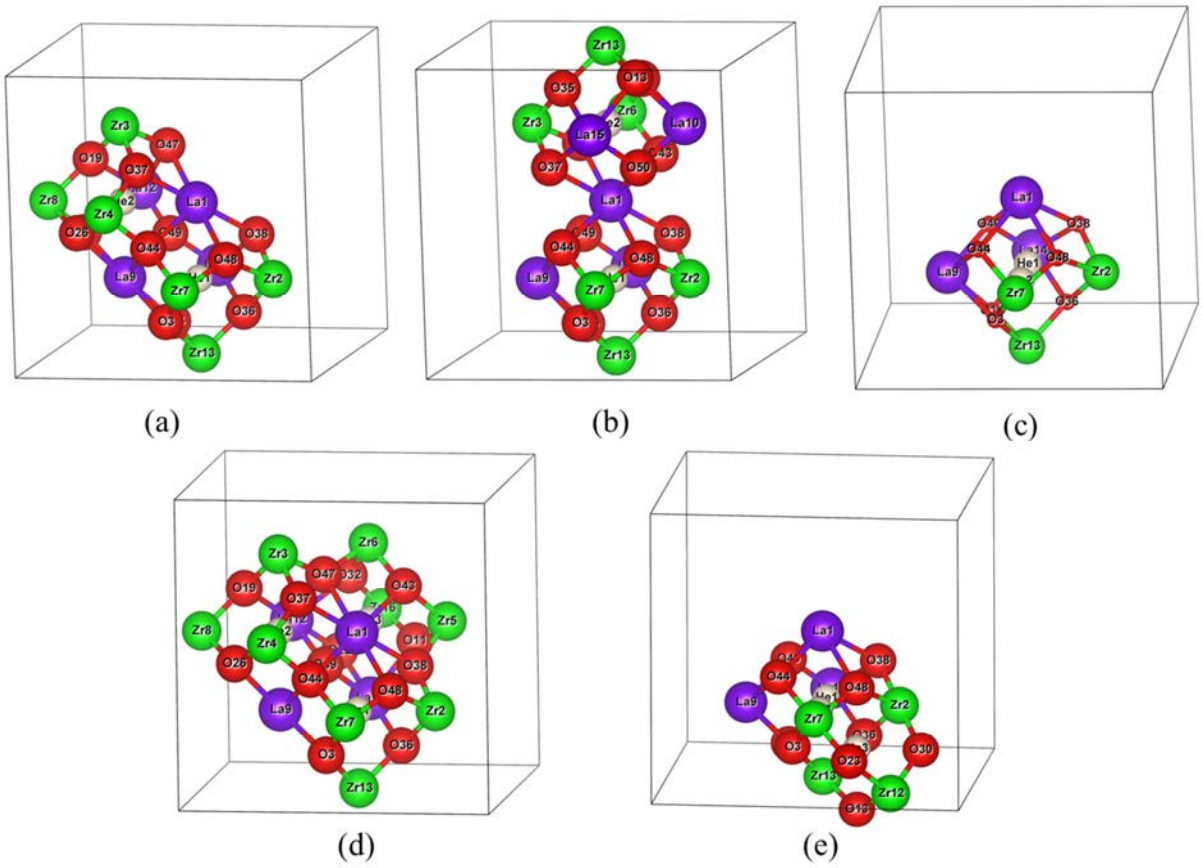

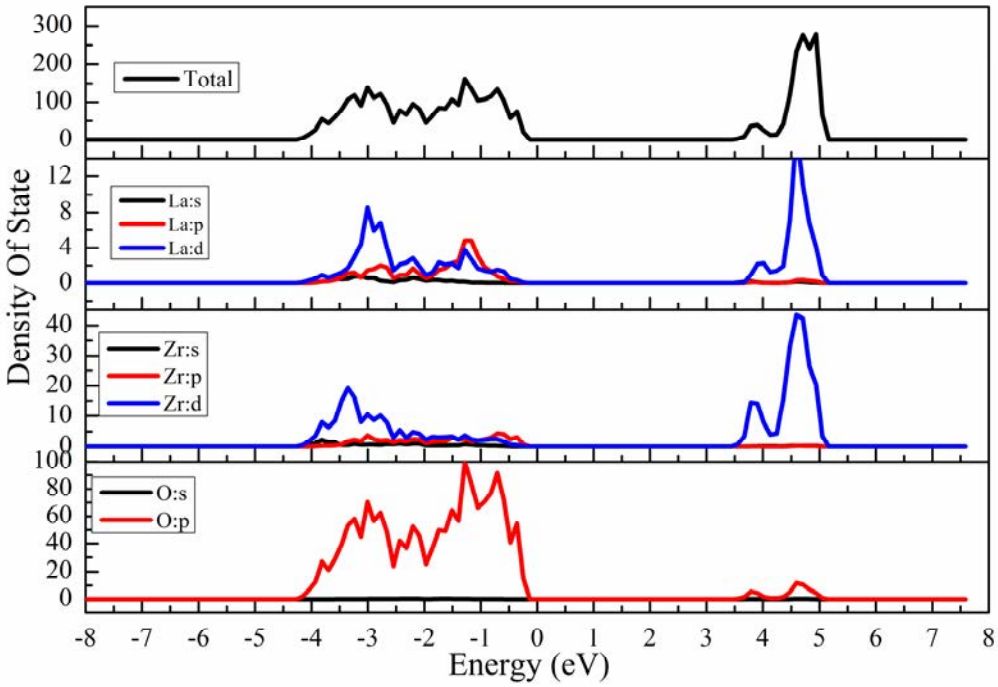

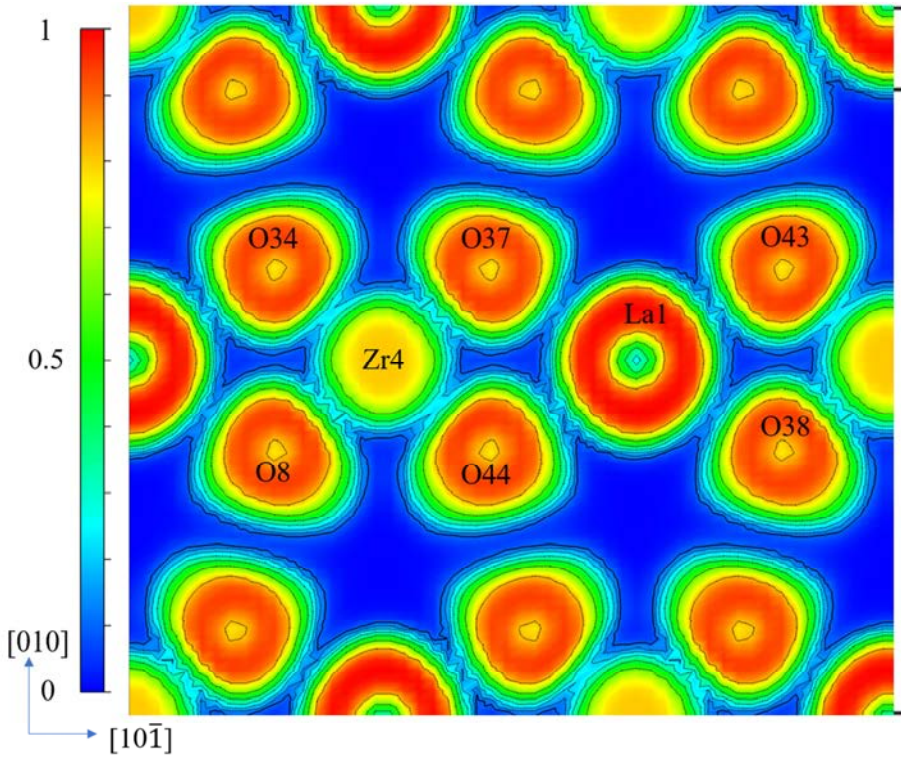

Ion	charge (e)
La1	8.8801
Zr4	9.4471
O8	7.3302
O34	7.3303
O37	7.3302
O38	7.3302
O43	7.3303
O44	7.3303

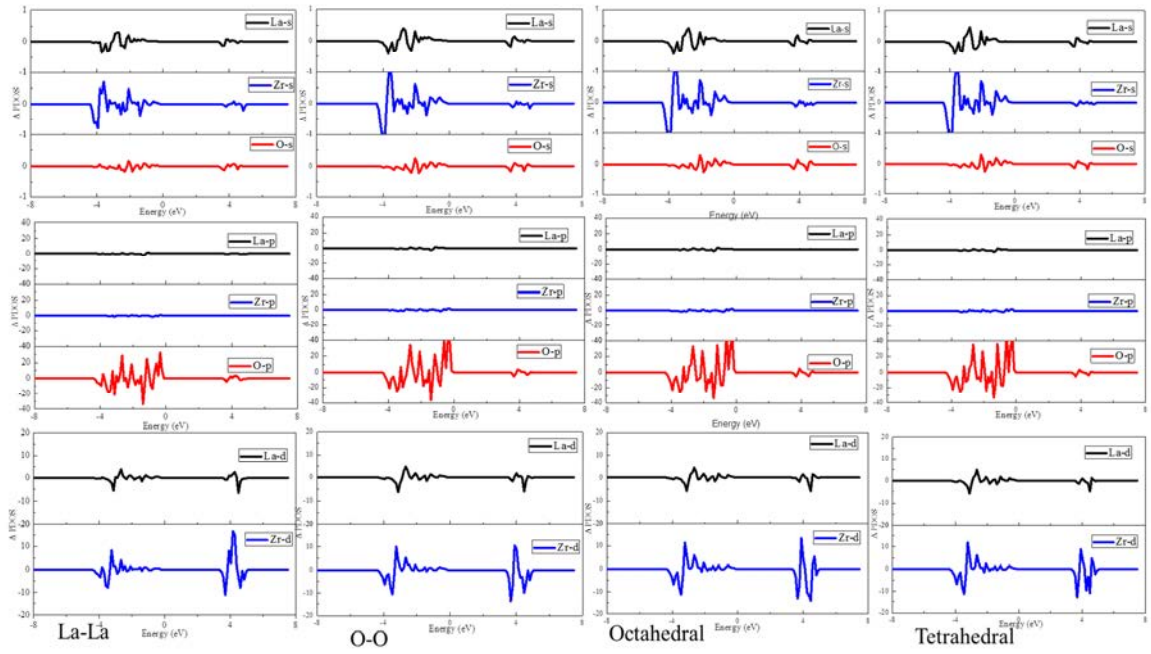

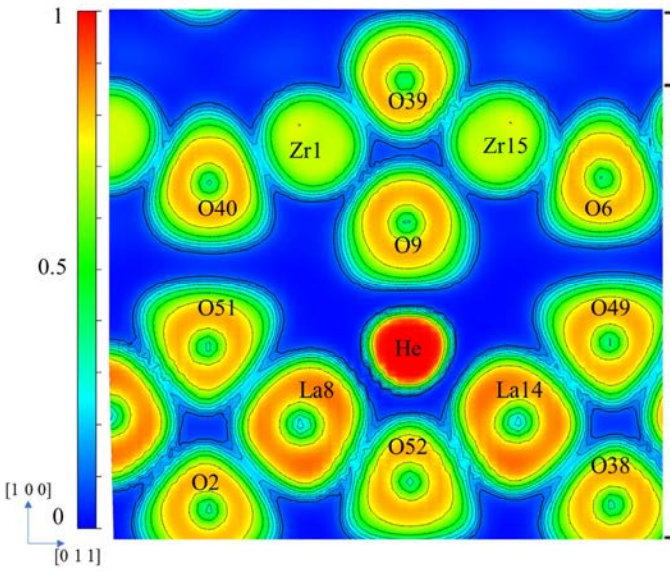

Ion	He-$La_2Zr_2O_7$		$La_2Zr_2O_7$	
	Charge (e)	Volume(pm^3)	Charge (e)	Volume(pm^3)
La8	8.9062	18272300	8.8801	18181500
La14	8.9061	18583500	8.8801	18181500
Zr1	8.9062	18272300	9.4474	11051400
Zr15	9.4390	10923800	9.4474	11051400
O2	7.3331	14482300	7.3302	14094000
O6	7.3446	15559200	7.3302	14094000
O9	7.3303	13894900	7.3302	14094000
O38	7.3302	14737700	7.3302	14094000
O39	7.3145	13145200	7.3302	14094000
O40	7.3194	14635500	7.3302	14094000
O49	7.3291	14652500	7.3636	14289400
O51	7.3256	14558700	7.3636	14289400
O52	7.3180	14030800	7.3636	14289400

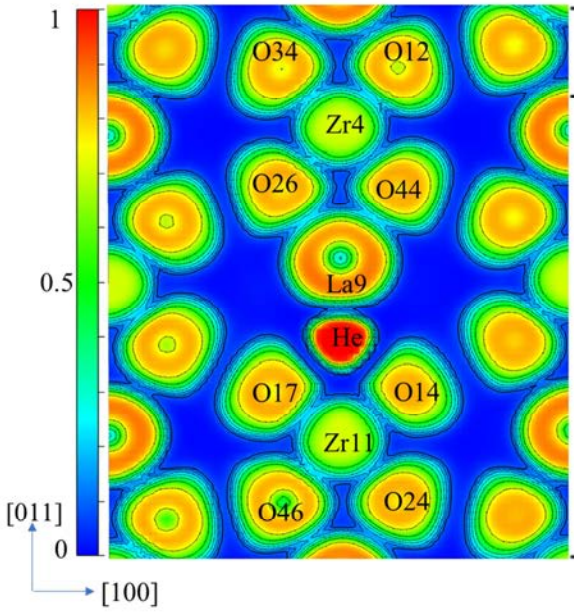

Ion	$He\text{-}La_2Zr_2O_7$		$La_2Zr_2O_7$	
	Charge (e)	Volume(pm^3)	Charge (e)	Volume(pm^3)
La9	8.8981	18953400	8.8801	18181500
Zr4	9.4317	11008400	9.4471	11041300
Zr11	9.4431	10977700	9.4471	11041300
O12	7.3343	14173000	7.3304	14101300
O14	7.3478	15669500	7.3304	14101300
O17	7.3359	14542200	7.3303	14097700
O24	7.3314	14667100	7.3303	14097700
O26	7.3238	14620500	7.3304	14101300
O34	7.3327	14526600	7.3303	14097700
O44	7.3324	14849800	7.3303	14097700
O46	7.3343	14173000	7.3304	14101300

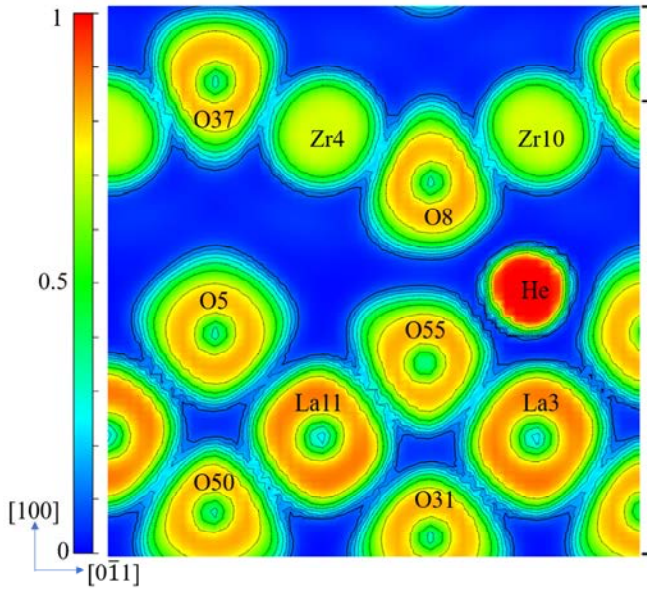

Ion	$He-La_2Zr_2O_7$		$La_2Zr_2O_7$	
	Charge (e)	Volume(pm^3)	Charge (e)	Volume(pm^3)
La3	8.8839	18620300	8.8801	18181500
La11	8.8998	18716200	8.8801	18181500
Zr4	9.4380	11020900	8.0978	11041300
Zr10	9.4384	11153300	9.4477	11061500
O5	7.3368	14605900	7.3302	14094000
O8	7.3335	14539000	7.3302	14094000
O31	7.3312	14564900	7.3302	14094000
O37	7.3337	14652900	7.3302	14094000
O50	7.3179	14395600	7.3636	14289400
O55	7.3495	14636500	7.3636	14289400

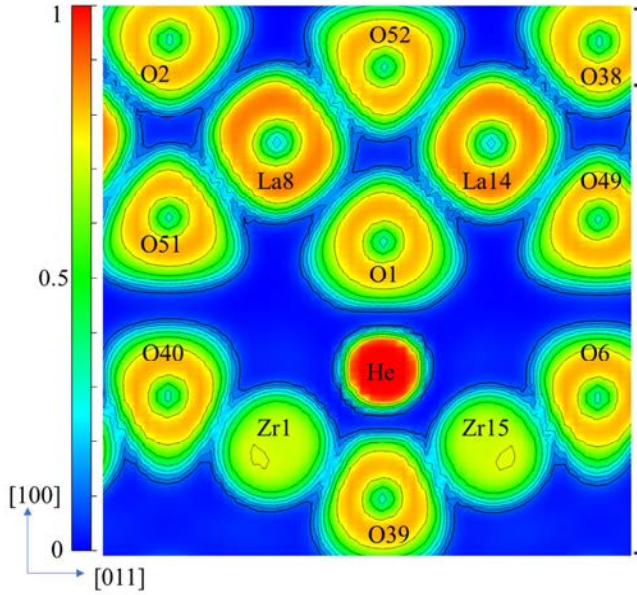

Ion	He-$La_2Zr_2O_7$		$La_2Zr_2O_7$	
	Charge (e)	Volume(pm^3)	Charge (e)	Volume(pm^3)
La8	8.8768	18530700	8.8801	18181500
La14	8.8768	18530700	8.8801	18181500
Zr1	9.4373	10952800	9.4474	11051400
Zr15	9.4373	10952800	9.4474	11051400
O1	7.3278	14067700	7.3302	14094000
O2	7.3306	14539900	7.3302	14094000
O6	7.3304	14465200	7.3302	14094000
O38	7.3305	14537000	7.3302	14094000
O39	7.3278	14067700	7.3302	14094000
O40	7.3304	14465200	7.3302	14094000
O49	7.3702	14823900	7.3636	14289400
O51	7.3702	14823900	7.3636	14289400
O52	7.3713	14680800	7.3636	14289400

Highlights

1. The existence of helium interstitial in $La_2Zr_2O_7$ may cause lattice swelling and the distortion of unit cell.
2. The octahedral interstitial site is the most stable helium interstitial site.
3. Low concentration of He interstitials may increase the radiation resistance of $La_2Zr_2O_7$ pyrochlore.
4. He absorptions in $La_2Zr_2O_7$ pyrochlore are weak repulsive and attractive chemical interactions.
5. <Zr-O> bonds play a more dominating role in determining the radiation tolerance of $La_2Zr_2O_7$.